Title: High-pressure speed of sound and related thermodynamic properties of N-alkylpyridinium bis(trifluoromethylsulfonyl)imides

Author: Małgorzata Musiał, Edward Zorębski, Michał Zorębski, Marzena Dzida

Citation style: Musiał Małgorzata, Zorębski Edward, Zorębski Michał, Dzida Marzena. (2020). High-pressure speed of sound and related thermodynamic properties of N-alkylpyridinium bis(trifluoromethylsulfonyl)imides. “Journal of Molecular Liquids” (Vol. 310 (2020), Art. No. 113188), doi 10.1016/j.molliq.2020.113188

Journal of Molecular Liquids 310 (2020) 113188

Contents lists available at ScienceDirect

Journal of Molecular Liquids

journal homepage: www.elsevier.com/locate/molliq

High-pressure speed of sound and related thermodynamic properties of *N*-alkylpyridinium bis(trifluoromethylsulfonyl)imides

Małgorzata Musiał [a,*], Edward Zorębski [b], Michał Zorębski [b], Marzena Dzida [b,*]

[a] Faculty of Science and Technology, August Chełkowski Institute of Physics, University of Silesia in Katowice, 75 Pulku Piechoty 1A, 41-500 Chorzow, Poland
[b] Faculty of Science and Technology, Institute of Chemistry, University of Silesia in Katowice, Szkolna 9, 40-006 Katowice, Poland

ARTICLE INFO

Article history:
Received 28 December 2019
Received in revised form 29 March 2020
Accepted 18 April 2020
Available online 28 April 2020

ABSTRACT

The speed of sound was measured in three *N*-alkylpyridinium bis(trifluoro-methylsulfonyl)imides containing cations with ethyl, butyl and hexyl chains at pressures up to 101 MPa over a temperature range from 293.15 to 323.15 K. This paper is the first reported direct measurement of the speed of sound in *N*-hexylpyridinium bis (trifluoro-methylsulfonyl)imide as a function of pressure and temperature at two frequencies (1.95 and 6.25 MHz), demonstrating the absence of ultrasonic velocity dispersion under experimental conditions. An acoustic method was used to determine the high-pressure density, isentropic compressibility, isothermal compressibility, isobaric thermal expansion, isobaric and isochoric heat capacities, and internal pressure. For the studied homologous series, the dependence of the speed of sound on the alkyl chain length of the pyridinium cation exhibits a minimum at both atmospheric and high pressures. With increasing pressure, the minimum becomes shallower and is shifted towards homologues with shorter carbon chains in the cation.

1. Introduction

There are few existing studies on the pressure (p) dependence of the speed of sound in ionic liquids (ILs) in contrast to the numerous studies that have been performed at atmospheric pressure [1]. The first investigations on the speed of sound in ILs as a function of the temperature T and pressure were carried out in 2005 [2,3] for imidazolium-based ILs. In 2006, Esperança et al. [4] investigated the speed of sound in two other imidazolium-based ILs. It was seven years before the next results on the high-pressure speed of sound were published by our group for an aprotic IL, 1-ethyl-3-methylimidazolium bis(trifluoromethylsulfonyl) imide ($[C_2C_1im][NTf_2]$) [5]. In a subsequent paper [6] we reported results on the high-pressure speed of sound in other 1-alkyl-3-methylimidazolium bis(trifluoromethylsulfonyl)imides ($[C_nC_1im][NTf_2]$, $n = 3$–6). In the abovementioned study, ultrasonic relaxation area was considered, and experimental p,T conditions appropriate for each of investigated homologues were used for the first time. Note that this procedure was adopted in all our subsequent studies [7–10], because only speed of sound outside the ultrasonic relaxation area can be used to correctly determine related thermodynamic properties via the Newton-Laplace relation. Skowronek et al. [6] reported consistent data for the $[C_nC_1im][NTf_2]$ series, which was used to determine how pressure affects the dependence of the speed of sound on the alkyl chain length of the cation $u(n)$. In aforementioned study, a comparison of $u(n)$ at atmospheric and high pressures showed that increasing the pressure shifts the minimum in $u(n)$ to homologues with lower alkyl chain lengths.

In this study, we investigate the speed of sound in three homologues of the *N*-alkylpyridinium bis(trifluoromethylsulfonyl)imide series $[C_npy][NTf_2]$ ($n = 2$, 4, 6) under pressures up to 101 MPa over the temperature range from 293.15 to 323.15 K with two objectives: first, to expand the database for the high-pressure speed of sound and related high-pressure thermodynamic quantities and second, to study the influence of pressure on the minimum in $u(n)$ that was recently detected at atmospheric pressure [11]. An acoustic method was used to determine $p\rho T$ and pC_pT data and related thermodynamic quantities (i.e. the isentropic compressibility, the isothermal compressibility, the isobaric thermal expansion, the isochoric heat capacity, and the internal pressure) based on experimental high-pressure results for the speed of sound and previous reports of the density and isobaric heat capacity at ambient pressure and temperatures ranging from 283.15 to 363.15 K and 293.15 to 323.15 K, respectively [11]. These data are invaluable because of the considerable potential application of pyridinium-based ILs for gas separation and absorption (especially for acid gases, such as SO_2 and CO_2) [12,13] and as working fluids [14]. Moreover, pyridinium-based ILs show higher biodegradability than imidazolium-based ILs [15], which is very important for environmental protection. Thus far, no $p\rho T$ data are available for any homologues of the $[C_npy][NTf_2]$ series, making the obtained results even

* Corresponding authors.
E-mail addresses: malgorzata.musial@smcebi.edu.pl (M. Musiał), marzena.dzida@us.edu.pl (M. Dzida).

https://doi.org/10.1016/j.molliq.2020.113188

more valuable. Note that Yebra et al. [16] recently reported $u(p,T)$ data for $[C_4py][NTf_2]$ but did not determine the related thermodynamic properties. It must be stressed that $p\rho T$ and pC_pT data, as well as all the related properties, obtained using the acoustic method (based on upT data) are highly reliable [10], unlike results based on experimentally determined $p\rho T$ data. The dependence of speed of sound on pressure can also be calculated from $p\rho T$ data [17–22], but the resulting agreement with experimental data is only qualitative in many cases [10]. These results are consistent with the general rule that integration procedures are more accurate than differentiation procedures. Moreover, it was recently shown [23] that thermodynamic properties obtained from $p\rho T$ data can be sometimes completely unreliable and even contradict the fundamental laws of thermodynamics.

2. Experimental

2.1. Materials

The $[C_npy][NTf_2]$ ($n = 2, 4, 6$) samples used in this study were purchased from Iolitec (Germany). The specifications of the ILs used in this study are provided in Table 1.

2.2. Speed of sound measurements

The pulse-echo-overlap method was used to determine the speed of sound at a frequency f of 2.75 MHz for an ambient pressure (u_0) and at a 1.95 MHz frequency at high pressures (u). The high-pressure speed of sound was also measured in $[C_6py][NTf_2]$ at 6.25 MHz. The measurements were performed at pressures up to 101 MPa or up to the freezing pressure (see Section 3.1). Two measuring cells with similar acoustic paths (ca. 30 mm) were used for the ambient and high-pressure measurements. Cells with a single-transducer and an acoustic mirror were used in both cases. The transmitting-receiving piezoceramic (PZT) transducer used in all our previous studies was employed for the atmospheric pressure measurements. However, in the high-pressure studies, a novel transmitting-receiving transducer, consisting of lithium niobate single crystal (gold plated) with tab coaxial electrodes, was used. The surface finish of the novel transducer enables operation at both the fundamental frequency and overtones. An arbitrary/function generator (Tektronix AFG 3051C) with high-frequency stability and small signal vibrations was also used. Apart from the aforementioned modifications, the same apparatus was used as in our previous studies, including the calibration and measurement procedures: details can be found elsewhere [24]. Re-distilled water with an electrolytic conductivity of $1\cdot10^{-4}\ \Omega^{-1}\cdot m^{-1}$ was used as a standard. The temperature was measured using a platinum resistance thermometer (Ertco Hart 850 with a PT100 probe traceable to a NIST standard) that was tested by a Fluke 1594A super-thermometer (a Pt probe with a nominal resistance of 25.5 Ω). The expanded uncertainty in the temperature measurement was estimated to be ±0.05 K. The combined expanded uncertainty in the speed of sound measurements within a 0.95 confidence interval was estimated to be better than $U(u_0) = \pm1\ m\cdot s^{-1}$ ($u_u = \pm 0.5\ m\cdot s^{-1}$, $k = 2$) at ambient pressure and $U(u) = \pm2\ m\cdot s^{-1}$($u_u = \pm 1\ m\cdot s^{-1}$, $k = 2$) at high pressure.

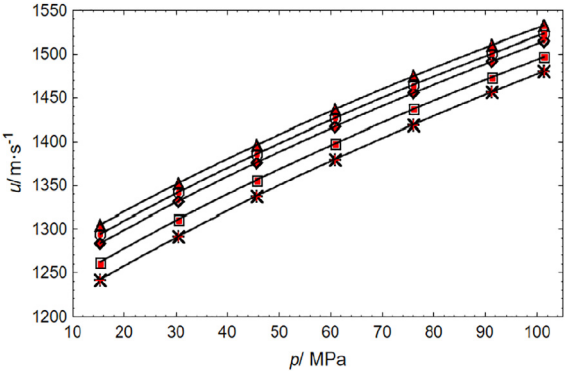

Fig. 1. Speed of sound u in $[C_6py][NTf_2]$ as a function of pressure p at different temperatures: 293.15 K (△, ▲); 298.15 K (○, ●); 303.15 K (◇, ◆); 313.15 K (□, ■); and 323.15 K (✱, ✚), where symbols (△, ○, ◇, □, ✱) and (▲, ●, ◆, ■, ✚) indicate measurement frequencies of 1.95 MHz and 6.25 MHz, respectively; lines are visual guides.

3. Results and discussion

3.1. Speed of sound at ambient and high pressures

We previously used classical ultrasound absorption to perform a preliminary analysis of the possible ultrasonic velocity dispersion areas in $[C_npy][NTf_2]$ homologues [11]. Note that the present study is the first confirmation of the absence of ultrasonic velocity dispersion under experimental conditions by direct measurement of the speed of sound in $[C_6py][NTf_2]$ as a function of pressure and temperature at two frequencies (1.95 and 6.25 MHz). The $[C_6py][NTf_2]$ was chosen for investigation, because the highest viscosity and classical ultrasound absorption have been demonstrated for this IL [11] among the investigated ILs. The results are shown in Fig. 1 and summarized in Table S1. In each case, the measured high-pressure speed of sound (at 1.95 and 6.25 MHz) do not differ by >2 $m\cdot s^{-1}$ (considering that the expanded uncertainty in the speed of sound measurement is ±2 $m\cdot s^{-1}$ at pressures up to 101 MPa), which confirms the absence of ultrasonic velocity dispersion in this frequency range and experimental conditions. However, this confirmation is only partial because of the relative closeness of the frequencies at which the phase speed of sound was measured, making it impossible to draw far-reaching conclusions, especially beyond the field of experimental conditions.

Although the aforementioned analysis for $[C_6py][NTf_2]$ enabled also the investigation of u in $[C_npy][NTf_2]$ ($n = 2, 4$) over the entire experimental available pressure and temperature range, i.e. up to 101 MPa over the temperature range from 293.15 to 323.15 K, the experimental u data for $[C_2py][NTf_2]$ and $[C_4py][NTf_2]$ are limited compared to those for $[C_6py][NTf_2]$ because of pressure-induced solidification. The experimental values are summarized in Table 2. A similar effect was previously observed for 1-ethyl-3-methylimidazolium methanesulfonate ($[C_2C_1im][C_1SO_3]$) [10], 1-alkyl-2,3-dimethylimidazolium bis(trifluoromethylsulfonyl)imides ($[C_nC_1C_1im][NTf_2]$, where $n = 2, 4$) [8], as well as for molecular organic liquids, such as methyl myristate [25], ethyl myristate [26], 1-

Table 1
Sample specifications.

IL	CAS	Molar mass/g·mol^{-1}	Purity/%	Water content/ppm	Halides[a]/ppm
$[C_2py][NTf_2]$	712354-97-7	388.31	>99	<100[a]/89[b]	<100
$[C_4py][NTf_2]$	187863-42-9	416.36	>99	<100[a]/60[b]	<100
$[C_6py][NTf_2]$	460983-97-5	444.41	>99	<200[a]/176[b]	<100

[a] Declared by supplier.
[b] Determined in this study using the Karl Fischer method (TitroLine 7500).

Table 2
Speed of sound[a] in [$C_n$py][NTf_2] at various temperatures T and pressures p.

T[b]/K	p[c]/MPa	u[d]/m·s^{-1}	T/K	p/MPa	u/m·s^{-1}	T/K	p/MPa	u/m·s^{-1}
[C_2py][NTf_2]								
293.15	0.101	1279.24	313.15	0.101	1235.42	318.15	75.99	1426.63
298.15	0.101	1268.06	313.15	15.20	1281.71	318.15	91.18	1460.18
303.15	0.101	1257.14	313.15	30.39	1324.87	318.15	101.32	1480.80
303.15	15.20	1302.61	313.15	45.59	1364.32	323.15	0.101	1214.32
303.15	30.39	1344.84	313.15	60.79	1401.61	323.15	15.20	1261.42
303.15	45.59	1383.58	313.15	75.99	1436.07	323.15	30.39	1304.78
308.15	0.101	1246.18	313.15	91.18	1469.37	323.15	45.59	1345.71
308.15	15.20	1292.27	313.15	101.32	1490.12	323.15	60.79	1382.69
308.15	30.39	1334.73	318.15	0.101	1224.89	323.15	75.99	1417.96
308.15	45.59	1373.63	318.15	15.20	1271.30	323.15	91.18	1451.54
308.15	60.79	1410.62	318.15	30.39	1314.68	323.15	101.32	1472.45
308.15	75.99	1444.94	318.15	45.59	1354.50			
308.15	91.18	1477.72	318.15	60.79	1391.84			
[C_4py][NTf_2]								
293.15	0.101	1256.72	303.15	60.79	1412.45	313.15	101.32	1488.60
293.15	15.20	1306.21	303.15	75.99	1449.05	318.15	0.101	1202.54
293.15	30.39	1351.64	303.15	91.18	1484.00	323.15	0.101	1192.24
298.15	0.101	1245.61	308.15	0.101	1223.76	323.15	15.20	1244.17
298.15	15.20	1295.42	313.15	0.101	1213.04	323.15	30.39	1291.24
298.15	30.39	1341.01	313.15	15.20	1263.71	323.15	45.59	1335.10
298.15	45.59	1383.13	313.15	30.39	1310.48	323.15	60.79	1375.57
298.15	60.79	1422.14	313.15	44.68	1351.03	323.15	75.99	1413.59
303.15	0.101	1234.64	313.15	56.77	1383.31	323.15	91.18	1449.28
303.15	15.20	1285.02	313.15	60.79	1393.75	323.15	101.32	1471.68
303.15	30.39	1330.80	313.15	75.99	1430.96			
303.15	45.59	1373.32	313.15	91.18	1466.17			
[C_6py][NTf_2]								
293.15	0.101	1251.33	298.15	91.18	1500.61	313.15	45.59	1356.14
293.15	15.20	1304.59	298.15	101.32	1523.66	313.15	60.79	1397.60
293.15	30.39	1352.38	303.15	0.101	1228.89	313.15	75.99	1437.14
293.15	45.59	1396.04	303.15	15.20	1283.45	313.15	91.18	1473.61
293.15	60.79	1436.71	303.15	30.39	1331.54	313.15	101.32	1496.99
293.15	75.99	1475.03	303.15	45.59	1376.17	318.15	0.101	1196.20
293.15	91.18	1510.26	303.15	60.79	1416.97	323.15	0.101	1185.70
293.15	101.32	1532.62	303.15	75.99	1455.64	323.15	15.20	1241.74
298.15	0.101	1240.08	303.15	91.18	1491.64	323.15	30.39	1291.53
298.15	15.20	1293.91	303.15	101.32	1514.99	323.15	45.59	1337.59
298.15	30.39	1341.81	308.15	0.101	1217.83	323.15	60.79	1379.80
298.15	45.59	1385.81	313.15	0.101	1206.95	323.15	75.99	1419.38
298.15	60.79	1426.78	313.15	15.20	1261.80	323.15	91.18	1456.65
298.15	75.99	1465.05	313.15	30.39	1311.03	323.15	101.32	1480.46

[a] Measured at 2.75 MHz at $p = 0.101$ MPa and 1.95 MHz at $p > 0.101$ MPa.
[b] $U(T) = 0.05$ K.
[c] $U(p) = 0.0015 \cdot p$ MPa.
[d] $U(u_0) = 1$ m·s^{-1} ($p = 0.101$ MPa); $U(u) = 2$ m·s^{-1} ($p > 0.101$ MPa).

decanol [27], and 1,4-butanediol [28]. The solidification phenomenon is related to relatively high melting temperatures T_m at atmospheric pressure (for example, 303.8 K and 292.80 K for [C_2C_1im][C_1SO_3] and 1,4-butanediol, respectively) and an increase of T_m with pressure. For the investigated homologues of [$C_n$py][NTf_2], the solid-liquid lines are shifted towards the p-axis (p-T diagram) with increasing n (according to T_m given below), i.e. in the order 2, 4 and 6. Although $T_m = 305.1$ K [14] or 303.6 K [29] for [C_2py][NTf_2], and $T_m = 299.1$ K [29] or 292 K [13] for [C_4py][NTf_2], the samples were in the liquid state at atmospheric pressure also below the aforementioned T_m, i.e. in the supercooled state. Several properties of [C_2py][NTf_2] and [C_4py][NTf_2] were investigated in this supercooled state (that is, at T below T_m) at atmospheric pressure, as has been previously reported [11]. These measurements were possible because ILs can be easily supercooled. In addition, several ILs are characterized by a considerable difference between T_m and the freezing temperature T_{fr}, i.e. there is a pronounced hysteresis between T_m and T_{fr}. The T_{fr} (at atmospheric pressure) for [C_2py][NTf_2] and [C_4py][NTf_2] is 252 K [14] and 224 K [30], respectively. The pressurization and, probably, so-called capillary effect lead to the solidification of [C_2py][NTf_2] and [C_4py][NTf_2] at evidently higher temperatures than T_{fr} at atmospheric pressure (the same behaviour was previously observed for [C_2C_1im][C_1SO_3] [10]). This effect is not relevant for [C_6py][NTf_2] because $T_m = 276.1$ K [31]. Note that the supercooling phenomenon generally refers to a non-equilibrium state. In addition, the thermal behaviour of ILs is rather complex and difficult to analyse. This behaviour results from the polymorphic nature of ILs in conjunction with the dependence of phase transitions on the cooling/heating method and/or the thermal history of the sample.

The speed of sound in [$C_n$py][NTf_2] measured under ambient pressure in this study is compared with literature data in Fig. 2a. The study results are in very good agreement with those reported by Dzida et al. [11], González et al. [32] and Benito et al. [33]. The relative deviations (Fig. 2a), *RDs* ($RD = 100\,(y_{\mathrm{exp}} - y_{lit})/y_{\mathrm{exp}}$), and absolute average relative deviations, *AARDs* ($AARD = (100/N)\sum_{i=1}^{n} |\,(y_{\mathrm{exp},\,i} - y_{lit,\,i})/y_{\mathrm{exp},\,i}|$, where N is the number of data points and y denotes u) between the our and literature studies are equal: −0.043 ÷ −0.026% ($AARD$ = 0.033%) [11]; −0.015 ÷ 0.011% ($AARD$ = 0.010%) [32]; −0.058 ÷ −0.010% ($AARD$ = 0.036%) [33] for [C_2py][NTf_2], and − 0.59 ÷ −0.32% ($AARD$ = 0.45%) [16] for [C_4py][NTf_2]. Note that the speed of sound at atmospheric pressure reported by Yebra et al. in the same paper [16] for other ILs ([C_4C_1pyr][NTf_2], [C_4C_1im][C_1SO_4], [C_4C_1im][TFO], and [C_4C_1im][$N(CN)_2$]) also deviates significantly from the

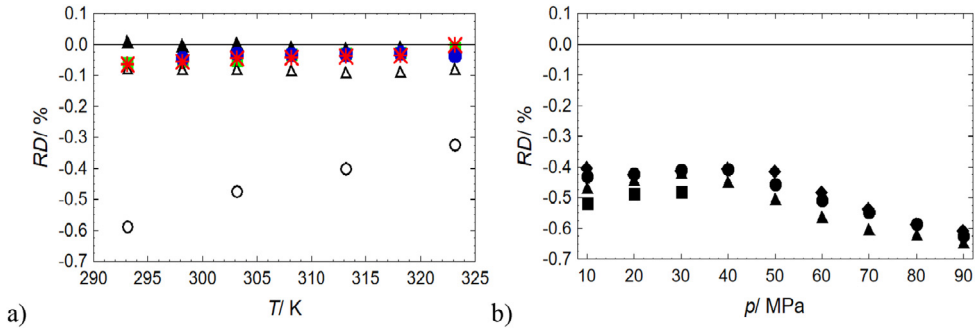

Fig. 2. Comparison of speed of sound obtained in this study with literature data: a) as a function of temperature T at atmospheric pressure in [C_2py][NTf_2] (■, [33]; ▲, [32]; ●, [11]); in [C_4py][NTf_2] (○, [16]; △, [11]); and in [C_6py][NTf_2] (✱, [11]); and b) as a function of pressure p in [C_4py][NTf_2] at temperatures of 293.15 K (■); 303.15 K (▲); 313.15 K (●); and 323.15 K (◆), [16].

available literature data from −1.7 to 0.09% [16] (corresponding to speed differences of 22.8 $m \cdot s^{-1}$ and 1.6 $m \cdot s^{-1}$, respectively). Yebra et al. also reported the speed of sound in [C_4py][NTf_2] under high-pressure (up to 95 MPa) for temperatures from 283.15 to 343.15 K [16]. The difference between the data of Yebra et al. and those obtained in this study at 293.15 K ranges from −0.52 (10 MPa) to −0.48% (30 MPa), while at 323.15 K ranges from −0.61 (90 MPa) to −0.40% (10 MPa) (Fig. 2b); $AARD = 0.49\%$. That is, the u values reported by Yebra et al. [16] are significantly higher (by up to 7.4 $m \cdot s^{-1}$) than those reported in this study. This result is indicative of a systematic error. Thus far, the speed of sound in [C_2py][NTf_2] and [C_6py][NTf_2] under high pressure has not been reported in the literature.

As in previous studies [5,6,8,10,24], the experimental data for the speed of sound at ambient pressure were approximated by polynomials of the form

$$u_0(T) = \sum_{i=0}^{2} a_i \cdot T^i, \tag{1}$$

and the data for speed of sound as a function of p and T were approximated by polynomials of the form

$$p - p_0 = \sum_{i=1}^{3} \sum_{j=0}^{2} a_{ij} (u - u_0)^i T^j. \tag{2}$$

The estimated coefficients a_i for the $u_0(T)$ dependence and the mean deviations δu_0 from the regression lines for [$C_n$py][NTf_2] are provided in Table S2, and the a_{ij} coefficients along with the mean deviations δu from the regression lines are given in Table S3.

3.2. Derived properties

The same calculation procedure was used as in our previous studies [6–8,10,24]. For [$C_n$py][NTf_2], the $u(p,T)$ values measured in this study were used together with our previously reported data for $\rho(T)$ and $C_p(T)$ at ambient pressure [11]. The $p\rho T$ and pC_pT data were determined at pressures and temperatures covering the p, T range of the u values measured in this study (Table 2). The estimated uncertainties in the density and isobaric heat capacity are ±0.02% and ±0.3%, respectively. The combined expanded uncertainties in the density and isobaric heat capacity within a 95% confidence interval are estimated to be better than $U(\rho) = 5 \cdot 10^{-4}$ $kg \cdot m^{-3}$ and $U(C_p) = 1.5 \cdot 10^{-2} \cdot C_p$, respectively. Further details can be found elsewhere [6,7,10]. The obtained density and molar isobaric heat capacity at high pressures are reported in Tables 3 and 4, respectively. Both ρ and C_p exhibit typical dependencies upon p and T over the range of study (ρ increases with p and decreases with T, whereas C_p increases with T and decreases extremely weakly with p). Additionally, the dependence of u on ρ is strictly linear along the isotherms (Fig. 3). The density data was correlated with p and T, using the form of Tait equation given below:

$$\rho(T,p) = \rho_0(T,p_0)/[1 - C \ \ln((p + B(T))/(p_0 + B(T)))], \tag{3}$$

where ρ_0 is the density at temperature T and ambient pressure $p_0 = 0.101325$ MPa; C is a temperature-independent coefficient; and $B(T)$ is a temperature-dependent coefficient, $B(T) = A_1 + A_2(T/100) + A_3(T/100)^2$, where A_1, A_2, and A_3 are adjustable parameters. The abovementioned coefficients are presented together with the standard deviations in Table S4.

Increasing the side chain length of the cation of the [$C_n$py][NTf_2] homologues leads to a decrease in the density. The non-linear $\rho(n)$ at

Table 3
Density ρ of [$C_n$py][NTf_2] at various temperatures T and pressures p.

p/MPa	ρ/kg·m^{-3} at T/K						
	293.15	298.15	303.15	308.15	313.15	318.15	323.15
[C_2py][NTf_2]							
0.101		1537.58[a]	1532.64[a]	1527.68[a]	1522.75[a]	1517.84[a]	1512.95[a]
10			1539.73	1534.90	1530.08	1525.29	1520.52
20			1546.57	1541.85	1537.14	1532.45	1527.79
30			1553.12	1548.49	1543.88	1539.29	1534.72
40			1559.41	1554.87	1550.35	1545.85	1541.37
50				1561.01	1556.57	1552.15	1547.75
60				1566.92	1562.56	1558.22	1553.89
70				1572.64	1568.35	1564.07	1559.82
80				1578.17	1573.95	1569.74	1565.55
90				1583.53	1579.37	1575.23	1571.11
100					1584.64	1580.56	1576.49
[C_4py][NTf_2]							
0.101	1453.26[a]	1448.39[a]	1443.74[a]	1439.13[a]	1434.50[a]	1429.87[a]	1425.25[a]
10	1460.28	1455.69	1451.11	1446.55	1442.00	1437.47	1432.96
20	1467.03	1462.54	1458.07	1453.62	1449.18	1444.76	1440.36
30	1473.47	1469.08	1464.71	1460.35	1456.01	1451.70	1447.40
40		1475.33	1471.05	1466.79	1462.54	1458.31	1454.10
50		1481.33	1477.14	1472.95	1468.79	1464.64	1460.52
60		1487.11	1482.99	1478.88	1474.80	1470.73	1466.68
70			1488.63	1484.60	1480.58	1476.58	1472.60
80			1494.08	1490.11	1486.17	1482.23	1478.32
90			1499.35	1495.45	1491.57	1487.70	1483.84
100				1500.63	1496.80	1492.99	1489.19
[C_6py][NTf_2]							
0.101	1387.69[a]	1383.14[a]	1378.62[a]	1374.12[a]	1369.64[a]	1365.18[a]	1360.73[a]
10	1394.74	1390.32	1385.92	1381.54	1377.18	1372.83	1368.50
20	1401.48	1397.17	1392.88	1388.61	1384.35	1380.11	1375.89
30	1407.89	1403.68	1399.49	1395.31	1391.16	1387.02	1382.90
40	1414.02	1409.90	1405.80	1401.71	1397.64	1393.59	1389.56
50	1419.90	1415.86	1411.84	1407.83	1403.84	1399.88	1395.92
60	1425.55	1421.58	1417.64	1413.71	1409.80	1405.90	1402.02
70	1430.99	1427.09	1423.22	1419.36	1415.52	1411.69	1407.89
80	1436.24	1432.41	1428.60	1424.81	1421.04	1417.28	1413.53
90	1441.32	1437.56	1433.81	1430.08	1426.37	1422.67	1418.98
100	1446.24	1442.54	1438.85	1435.18	1431.52	1427.88	1424.26

[a] Data reported previously in [11].

Table 4
Molar isobaric heat capacity C_p of [$C_n$py][NTf_2] at various temperatures T and pressures p.

p/MPa	C_p/J·mol^{-1}·K^{-1} at T/K						
	293.15	298.15	303.15	308.15	313.15	318.15	323.15
[C_2py][NTf_2]							
0.101	476.6[a]	478.6[a]	480.8[a]	483.2[a]	485.7[a]	488.4[a]	491.3[a]
10			480.6	482.9	485.5	488.1	491.0
20			480.4	482.7	485.2	487.9	490.8
30			480.2	482.6	485.1	487.8	490.6
40			480.1	482.4	484.9	487.6	490.5
50				482.3	484.8	487.5	490.4
60				482.2	484.7	487.4	490.3
70				482.1	484.6	487.3	490.2
80				482.1	484.6	487.3	490.2
90				482.0	484.5	487.2	490.1
100					484.5	487.2	490.1
[C_4py][NTf_2]							
0.101	537.6[a]	540.2[a]	543.0[a]	545.9[a]	549.1[a]	552.5[a]	556.1[a]
10	537.4	539.9	542.7	545.6	548.8	552.2	555.8
20	537.1	539.7	542.4	545.4	548.6	551.9	555.5
30	536.9	539.5	542.2	545.2	548.4	551.7	555.3
40		539.3	542.1	545.0	548.2	551.5	555.1
50		539.1	541.9	544.9	548.0	551.4	555.0
60		539.0	541.8	544.7	547.9	551.3	554.8
70			541.6	544.6	547.8	551.1	554.7
80			541.5	544.5	547.7	551.0	554.6
90			541.4	544.4	547.5	550.9	554.5
100				544.3	547.4	550.8	554.4
[C_6py][NTf_2]							
0.101	596.6[a]	599.5[a]	602.6[a]	605.9[a]	609.4[a]	613.0[a]	616.9[a]
10	596.3	599.2	602.3	605.6	609.0	612.7	616.5
20	596.1	599.0	602.0	605.3	608.8	612.4	616.3
30	595.8	598.7	601.8	605.1	608.6	612.2	616.1
40	595.7	598.6	601.7	604.9	608.4	612.0	615.9
50	595.5	598.4	601.5	604.8	608.2	611.9	615.7
60	595.4	598.3	601.4	604.7	608.1	611.8	615.6
70	595.3	598.2	601.3	604.5	608.0	611.6	615.5
80	595.2	598.1	601.2	604.4	607.9	611.5	615.4
90	595.1	598.0	601.1	604.3	607.8	611.4	615.3
100	595.0	597.9	601.0	604.2	607.7	611.4	615.2

[a] Data reported previously in [11].

0.101 MPa makes density increments not constant. Increasing the pressure systematically shifted the density of the three tested homologues: thus, most likely, the same $\rho(n)$ dependence is expected to occur at 100 MPa. At 318.15 K, the density of all studied [$C_n$py][NTf_2] similarly decreases by approximately 10% at both 0.101 MPa and 100 MPa (Fig. 4).

The isentropic compressibility κ_S was obtained using the Newton-Laplace formula:

$$\kappa_S = \rho^{-1} \cdot u^{-2}. \quad (4)$$

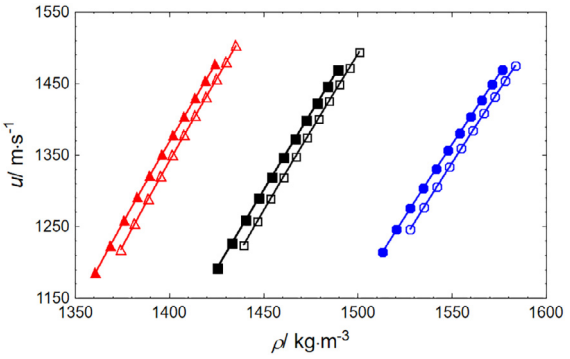

Fig. 3. Speed of sound u as a function of density ρ for [C_2py][NTf_2] (○, ●), [C_4py][NTf_2] (□, ■), and [C_6py][NTf_2] (△, ▲); empty symbols denote 308.15 K, and filled symbols denote 323.15 K. Lines are visual guides.

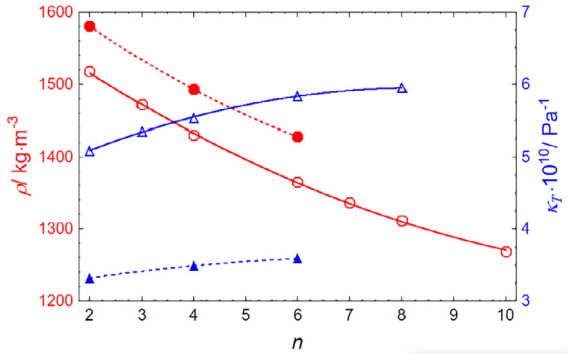

Fig. 4. Dependence of density and isothermal compressibility on alkyl chain length of cation, $\rho(n)$ and $\kappa_T(n)$, for [$C_n$py][NTf_2] at 318.15 K: at 0.101 MPa, ρ (○: n = 2,3,4,6,8 [11] and n = 7,10 [13]) and κ_T (△, [11]); and at 100 MPa (this study), ρ (●) and κ_T (▲); approximate fits at 0.101 MPa are $\rho(n) = 1613.1 - 52.454 \cdot n + 1.822 \cdot n^2$ and $\kappa_T(n) = 4.4518 + 0.3611 \cdot n - 0.0218 \cdot n^2$ with correlation coefficients R above 0.9995; lines at 100 MPa are visual guides only.

The expanded uncertainty in the isentropic compressibility within a 95% confidence interval is estimated to be better than $U(\kappa_S) = 1 \cdot 10^{-2}\ \kappa_S$. The κ_S values of [$C_n$py][NTf_2] (n = 2, 4, 6) range from $4.0445 \cdot 10^{-10}$ to $5.2277 \cdot 10^{-10}$ Pa^{-1} at 0.101 MPa and clearly decrease by approximately 22–38% from 0.101 to 100 MPa for temperatures from 293.15 to 323.15 K (Table S5). The isentropic compressibility increases with the alkyl chain length for the [$C_n$py][NTf_2] series, confirming previous observations for [$C_n C_1$im][NTf_2], [$C_n C_1$im][NTf_2], and the 1-alkyl-1-methylpyrrolidinium [$C_n C_1$pyr][NTf_2] series [8]. The κ_S values of [C_4py][NTf_2] and [$C_4 C_1$pyr][NTf_2] are similar for all pressures (Fig. 5a), i.e., the differences among the κ_S values do not exceed 0.3% at 0.101 MPa and slightly increase to 0.8% at 100 MPa, independent of the temperature. The κ_S values for imides generally increase for cations in the following order: $[C_4C_1C_1im]^+ < [C_4py]^+ \approx [C_4C_1pyr]^+ < [C_4C_1im]^+$. However, the structural differences between the aromatic pyridinium ring and the non-aromatic pyrrolidinium ring do not affect the macroscopic κ_S.

The isobaric thermal expansion $\alpha_p \equiv -(1/\rho)(\partial\rho/\partial T)_p$ had an expanded uncertainty of $U(\alpha_p) = 1 \cdot 10^{-2}\ \alpha_p$ (within a 95% confidence interval), and the results are shown in Table S6. The values of α_p for [$C_n$py]

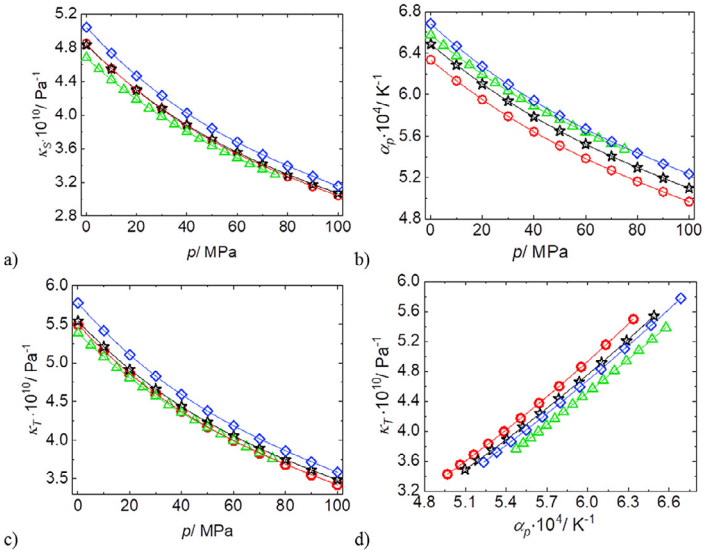

Fig. 5. Pressure dependence at 318.15 K of (a) isentropic compressibility κ_S, (b) isobaric thermal expansion α_p, (c) isothermal compressibility κ_T, and (d) isothermal compressibility κ_T as a function of isobaric thermal expansion α_p at 318.15 K for different ILs: [C_4py][NTf_2] (☆, this study); [$C_4 C_1$pyr][NTf_2] (○, [7]; and [$C_4 C_1$im][NTf_2] (◇, [6]); [$C_4C_1C_1$im][NTf_2] (△, [8]); lines are visual guides.

$[NTf_2]$ ($n = 2, 4, 6$) are almost temperature-independent and nearly equal, ranging from $6.469 \cdot 10^{-4}$ to $6.530 \cdot 10^{-4}$ K^{-1} at 0.101 MPa [11] and from $5.08 \cdot 10^{-4}$ to $5.16 \cdot 10^{-4}$ K^{-1} at 100 MPa for temperatures from 293.15 to 323.15 K (Table S6). As Fig. 5b shows, among the compared ILs with the $[NTf_2]^-$ anion, the highest and lowest α_p values are found for $[C_4C_1im][NTf_2]$ and $[C_4C_1pyr][NTf_2]$, respectively. At 318.15 K, the differences between the highest and lowest α_p values are 5.5% and 5.3% under pressures of 0.101 MPa and 100 MPa, respectively.

The isothermal compressibility, κ_T, the molar isochoric heat capacity, C_V, and the internal pressure, p_{int}, were obtained using the following formulas:

$$\kappa_T = \kappa_S + T \cdot V_m \cdot \alpha_p^2 \cdot {C_p}^{-1}, \tag{5}$$

$$C_V = C_p - T \cdot V_m \cdot \alpha_p^2 / \left(\rho^{-1} \cdot u^{-2} + T \cdot V_m \cdot \alpha_p^2 \cdot {C_p}^{-1}\right), \tag{6}$$

$$P_{int} = \left[T \cdot \alpha_p / \left(\rho^{-1} \cdot u^{-2} + T \cdot V_m \cdot \alpha_p^2 \cdot {C_p}^{-1}\right)\right] - p, \tag{7}$$

where V_m is the molar volume. The values of κ_T, C_V and P_{int} are summarized in Tables S7, S8, and S9, respectively. The expanded uncertainties in κ_T, C_V and P_{int} within a 95% confidence interval are estimated to be better than $U(\kappa_T) = 1 \cdot 10^{-2}$ κ_T Pa^{-1}, $U(C_V) = 2 \cdot 10^{-2} C_V$ $J \cdot mol^{-1} \cdot K^{-1}$ and $U(P_{int}) = 1 \cdot 10^{-2}$ P_{int} MPa, respectively. The κ_T values of the investigated pyridinium-based ILs vary from $4.703 \cdot 10^{-10}$ to $5.957 \cdot 10^{-10}$ Pa^{-1} at temperatures ranging from 293.15 to 323.15 K at 0.101 MPa. Increasing the pressure up to 100 MPa, results in a 34–39% decrease in κ_T. Increasing the side chain length of the cation in the $[C_npy][NTf_2]$ homologues leads to an increase in κ_T. At 0.101 MPa, the $\kappa_T(n)$ dependence is non-linear, i.e. the κ_T increments are not constant. At 100 MPa, a similar but weaker trend is observed (Fig. 4). Similarly as for κ_S, the κ_T values for $[C_4py][NTf_2]$ and $[C_4C_1pyr][NTf_2]$ are similar for all pressures (Fig. 5c). The difference in κ_T between the two abovementioned ILs is 0.8% at 0.101 MPa and increases to 1.8% at 100 MPa, independent of the temperature: this difference is slightly higher than that for κ_S. The κ_T values for the four $[NTf_2]^-$ anion-based ILs increase in the following order: $[C_4C_1C_1im]^+ < [C_4C_1pyr]^+ < [C_4py]^+ < [C_4C_1im]^+$. The relationship between α_p and κ_T at 318.15 K is shown in Fig. 5d for these four ILs.

Under ambient pressure, C_V varies from 411.6 $J \cdot mol^{-1} \cdot K^{-1}$ for $[C_2py][NTf_2]$ to 541.3 $J \cdot mol^{-1} \cdot K^{-1}$ for $[C_6py][NTf_2]$ for temperatures ranging from 293.15 to 323.15 K. Increasing the pressure up to 100 MPa causes a slight decrease of 0.4–0.8% in C_V along the isotherms for the investigated ILs (Table S8). These trends are similar to those observed for C_p (i.e., a 0.25–0.30% decrease along the isotherms, see Table 4). Thus, both C_p and C_V show typical behaviour over the investigated p,T range behaviour, i.e. $(\partial C_p/\partial T)_p$ and $(\partial C_V/\partial T)_p$ are positive, $(\partial C_p/\partial p)_T$ and $(\partial C_V/\partial p)_T$ are negative, and the absolute values of their partial derivatives are related as follows: $|(\partial C_p/\partial T)_p| > |(\partial C_p/\partial p)_T|$ and $|(\partial C_V/\partial T)_p| > |(\partial C_V/\partial p)_T|$. That is, p influences the heat capacity less than T over the investigated p,T range.

In Fig. 6a, b and c, the isotherms of $P_{int}(p)$ are non-monotonic and intersect at approximately 100 MPa for $[C_2py][NTf_2]$ and at approximately 80 MPa for $[C_4py][NTf_2]$ and $[C_6py][NTf_2]$. The maxima of the $P_{int}(p)$ isotherms for $[C_2py][NTf_2]$, $[C_4py][NTf_2]$ and $[C_6py][NTf_2]$ range from 10–30 MPa, 15–35 MPa and 20–40 MPa, respectively. The maxima of the isotherms, i.e., the points at which $(\partial P_{int}/\partial p)_T = 0$, for each homologue are shifted towards higher pressure for increasing T. At the intersection of the $P_{int}(p)$ isotherms and in the vicinity, P_{int} is independent of T, i.e. $(\partial P_{int}/\partial T)_p \approx 0$, whereas $(\partial P_{int}/\partial T)_p < 0$ at lower pressures and $(\partial P_{int}/\partial T)_p > 0$ at higher pressures. The $[C_2py][NTf_2]$ is an exception because the isotherms intersection occurs at the maximal experimentally available pressure of 100 MPa. The crossing points for the $P_{int}(p)$ isotherms are not unusual. Such crossing points (or in some cases, regions, to be more precise), at which isotherms of $P_{int}(p)$ intersect each other, have been observed repeatedly for both ILs [34,35] and molecular liquids [27,36]. The same considerations apply to the maxima of the isotherms of $P_{int}(p)$ [25–27,34–36]. A detailed discussion of the similarities between ILs and molecular liquids relating $P_{int}(p,T)$ to intermolecular interactions can be found in our recently published article [35].

The dependence of P_{int} on p and T for pyridinium-based imides is similar to those reported for di-substituted imidazolium-based imides [35]. A comparison of $P_{int}(p)$ at 318.15 K for imides with pyridinium, pyrrolidinium, di- and tri-substituted imidazolium cations with butyl

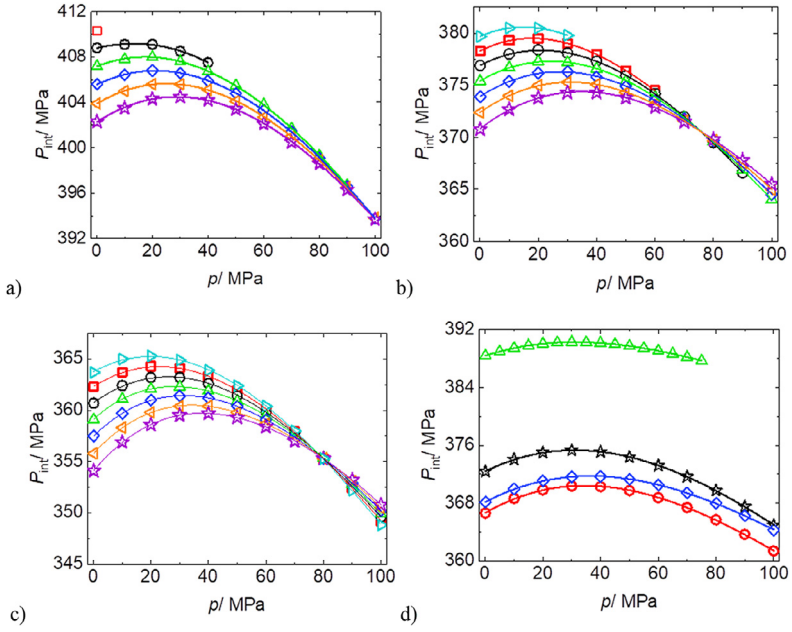

Fig. 6. Internal pressure P_{int} as a function of pressure p for a) $[C_2py][NTf_2]$, b) $[C_4py][NTf_2]$, and c) $[C_6py][NTf_2]$ at different temperatures: 293.15 K (▷), 298.15 K (□), 303.15 K (○), 308.15 K (△), 313.15 K (◇), 318.15 K (◁), and 323.15 K (☆), and d) P_{int} as a function of pressure p at 318.15 K for different ILs: $[C_4py][NTf_2]$ (☆, this study); $[C_4C_1pyr][NTf_2]$ (○, [7]); $[C_4C_1im][NTf_2]$ (◇, [6]); and $[C_4C_1C_1im][NTf_2]$ (△, [8]); lines are visual guides.

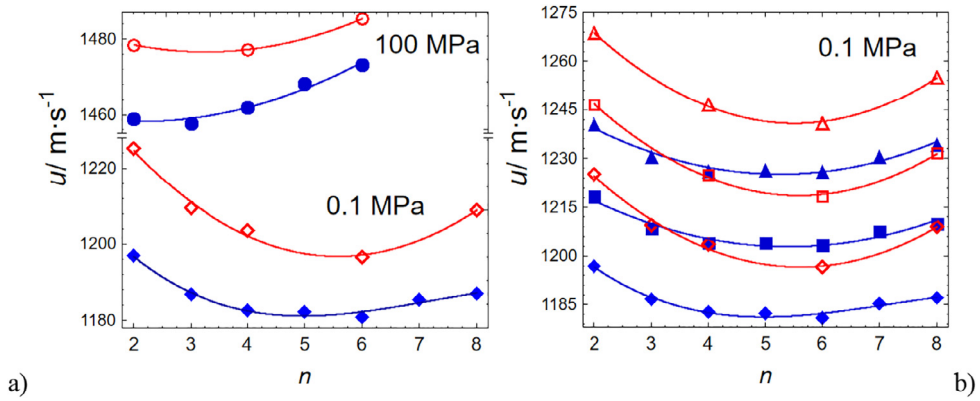

Fig. 7. Speed of sound as a function of alkyl chain length of cation for $[C_npy][NTf_2]$ (red open symbols) and $[C_nC_1im][NTf_2]$ [6,37] (blue filled symbols) at a) 318.15 K at 0.101 MPa (◇, ◆; [11] and [6], respectively) and 100 MPa (○, ●; this study and [37], respectively); and b) ambient pressure [6,11] at: 298.15 K (△, ▲); 308.15 K (□, ■); and 318.15 K (◇, ◆); lines are visual guides. (For interpretation of the references to color in this figure legend, the reader is referred to the web version of this article.)

side alkyl chains is shown in Fig. 6d. The highest P_{int} is observed for $[C_4C_1C_1im][NTf_2]$, and the lowest P_{int} is observed for $[C_4C_1pyr][NTf_2]$: the differences between the highest and lowest values at 318.15 K vary from 5.4 to 5.9% for pressures ranging from 0.101 to 75 MPa. The maxima of the $P_{int}(p)$ isotherms range from 30 to 40 MPa for all the considered ILs (Fig. 6d).

3.3. Minimum of u(n) dependence

The obtained results for $[C_npy][NTf_2]$ indicate that as the pressure increases, the minimum of $u(n)$ is shifted towards an IL containing a cation with a shorter carbon chain (Fig. 7a) but is not affected by temperature (over the investigated range) irrespective of the pressure (Fig. 7b shows the results at atmospheric pressure). The minimum of $u(n)$ for the $[C_npy][NTf_2]$ series occurs at ambient pressure for $n = 6$ [11] and is shifted towards a homologue with lower n at 100 MPa, most likely $n = 3$ (Fig. 7a): however, this minimum is very shallow in comparison to those at ambient pressures. The obtained results are consistent with previously reported observations for the $[C_nC_1im][NTf_2]$ series [6], wherein a very shallow minimum was observed at 100 MPa within the range of uncertainty (see Fig. 7).

Our research on ILs to date leads to the hypothesis that a minimum in $u(n)$ is only exhibited in ILs with a $[NTf_2]^-$ anion. The limitations associated with the acoustic experiment [1] and melting points, which often change significantly with the length of the carbon chain of a cation, make it difficult to systematically analyse the impact of the chain length and the pressure on the speed of sound in series of ILs. A fairly complete analysis is only possible for two homologous series, i.e. $[C_npy][NTf_2]$ and $[C_nC_1im][NTf_2]$: for both the $[C_nC_1C_1im][NTf_2]$ and $[C_nC_1pyr][NTf_2]$ series, data is only available for two homologues [7,8], which precludes analysis of the entire series. However, the inversion of the speed of sound has at least been observed for the $[C_nC_1C_1im][NTf_2]$ and $[C_nC_1pyr][NTf_2]$ series, i.e., the speed of sound at atmospheric pressure is higher in homologues containing cations with shorter alkyl chains than those with longer alkyl chains, whereas the speed of sound under high pressures is lower for homologues containing cations with shorter alkyl chains than those with longer alkyl chains – this effect has been described in detail in our previous studies [7,8].

4. Summary

The speed of sound in $[C_npy][NTf_2]$ ($n = 2, 4, 6$) was measured at pressures up to 101 MPa (or up to near the freezing pressure) and temperatures ranging from 293.15 to 323.15 K. The consistency among the upT, ρpT (which is also reported in the Tait equation form) and C_ppT data enabled related thermodynamic properties to be determined, i.e., the isentropic compressibility, the isothermal compressibility, the isobaric thermal expansion, the isochoric heat capacity, and the internal pressure, over the entire p, T range of the speed of sound investigations. The minimum in $u(n)$ observed at atmospheric pressure for $n = 6$ [11] also occurs at high pressures but is shifted towards homologues with shorter side alkyl chains of the cation, most likely to $n = 3$ under 100 MPa. However, the minimum at high pressure is very shallow in comparison to that at atmospheric pressure.

CRediT authorship contribution statement

Małgorzata Musiał: Investigation, Data curation, Visualization, Writing - original draft.**Edward Zorębski:**Conceptualization, Writing - review & editing, Visualization.**Michał Zorębski:**Investigation, Methodology, Validation, Software.**Marzena Dzida:**Conceptualization, Writing - review & editing, Supervision.

Declaration of competing interest

The authors declare that they have no known competing financial interests or personal relationships that could have appeared to influence the work reported in this paper.

Appendix A. Supplementary data

The Supporting information presents 9 Tables containing the following information: the (a_i), (a_{ij}), and (C, A_1, A_2, A_3) coefficients for Eqs. (1), (2), and (3), respectively; the speed of sound u in $[C_6py][NTf_2]$ at a frequency of 6.25 MHz; the isobaric thermal expansion; the isentropic compressibility; the molar isochoric heat capacity; the isothermal compressibility; and the internal pressure. Supplementary data to this article can be found online at https://doi.org/10.1016/j.molliq.2020.113188.

References

[1] M. Dzida, E. Zorębski, M. Zorębski, M. Żarska, M. Geppert-Rybczyńska, M. Chorążewski, J. Jacquemin, I. Cibulka, Speed of sound and ultrasound absorption in ionic liquids, Chem. Rev. 117 (2017) 3883–3929.
[2] R. Gomes de Azevedo, J.M.S.S. Esperança, J. Szydlowski, Z.P. Visak, P.F. Pires, H.J.R. Guedes, L.P.N. Rebelo, Thermophysical and thermodynamic properties of ionic liquids over an extended pressure range: [Bmim][NTf2] and [Hmim][NTf2], J. Chem. Thermodyn. 37 (2005) 888–899.
[3] R. Gomes de Azevedo, J.M.S.S. Esperança, V. Najdanovic-Visak, Z.P. Visak, H.J.R. Guedes, M. Nunes da Ponte, L.P.N. Rebelo, Thermophysical and thermodynamic properties of 1–butyl–3–methylimidazolium tetrafluoroborate and 1–butyl–3–methylimidazolium hexafluorophosphate over an extended pressure range, J. Chem. Eng. Data 50 (2005) 997–1008.
[4] J.M.S.S. Esperança, Z.P. Visak, N.V. Plechkova, K.R. Seddon, H.J.R. Guedes, L.P.N. Rebelo, Density, speed of sound, and derived thermodynamic properties of ionic liquids over an extended pressure range. 4. [C3mim][NTf2] and [C5mim][NTf2], J. Chem. Eng. Data 51 (2006) 2009–2015.

[5] M. Dzida, M. Chorążewski, M. Geppert-Rybczyńska, E. Zorębski, M. Zorębski, M. Żarska, B. Czech, Speed of sound and adiabatic compressibility of 1-ethyl-3-methylimidazolium bis(trifluoromethylsulfonyl)imide under pressures up to 100 MPa, J. Chem. Eng. Data 58 (2013) 1571–1576.
[6] J. Skowronek, M. Dzida, E. Zorębski, M. Chorążewski, S. Jężak, M. Żarska, M. Zorębski, J. Jacquemin, P. Goodrich, High pressure speed of sound and related thermodynamic properties of 1-ethyl-3-methylimidazolium bis[(trifluoromethyl)sulfonyl] imides (from 1-propyl- to 1-hexyl-), J. Chem. Eng. Data 61 (2016) 3794–3805.
[7] M. Musiał, K. Malarz, A. Mrozek-Wilczkiewicz, R. Musiol, E. Zorębski, M. Dzida, Pyrrolidinium-based ionic liquids as sustainable media in heat transfer processes, ACS Sustain. Chem. Eng. 5 (2017) 11024–11033.
[8] M. Musiał, M. Kuczak, A. Mrozek-Wilczkiewicz, R. Musiol, E. Zorębski, M. Dzida, Tri-substituted imidazolium-based ionic liquids as innovative heat transfer media in sustainable energy systems, ACS Sustain. Chem. Eng. 6 (2018) 7960–7968.
[9] M. Dzida, M. Musiał, E. Zorębski, S. Jężak, J. Skowronek, K. Malarz, A. Mrozek-Wilczkiewicz, R. Musiol, J. Skowronek, A. Cyranka, M. Świątek, M. Piński, Comparative study of the high pressure thermophysical properties of 1-ethyl-3-methylimidazolium and 1,3-diethylimidazolium ethyl sulfates for use as sustainable and efficient hydraulic fluids, ACS Sustain. Chem. Eng. 6 (2018) 10934–10943.
[10] M. Musiał, M. Zorębski, M. Dzida, J. Safarov, E. Zorębski, E. Hassel, High pressure speed of sound and related properties of 1-ethyl-3-ethylimidazolium methanesulfonate, J. Mol. Liq. 276 (2019) 885–896.
[11] M. Dzida, M. Musiał, E. Zorębski, M. Zorębski, J. Jacquemin, P. Goodrich, Z. Wojnarowska, M. Paluch, Comparative study of effect of alkyl chain length on thermophysical characteristics of five *N*-alkylpyridinium bis (trifluoromethylsulfonyl)imides with imidazolium-based ionic liquids, J. Mol. Liq. 278 (2019) 401–412.
[12] S. Zeng, H. Gao, X. Zhang, H. Dong, X. Zhang, S. Zhang, Efficient and reversible capture of SO_2 by pyridinium-based ionic liquids, Chem. Eng. J. 251 (2014) 248–256.
[13] S. Zeng, J. Wang, L. Bai, B. Wang, H. Gao, D. Shang, X. Zhang, S. Zhang, Highly selective capture of CO_2 by ether-functionalized pyridinium ionic liquids with low viscosity, Energy Fuel 29 (2015) 6039–6048.
[14] M. Villanueva, J.J. Parajó, P.B. Sánchez, J. García, J. Salgado, Liquid range temperature of ionic liquids as potential working fluids for absorption heat pumps, J. Chem. Thermodyn. 91 (2015) 127–135.
[15] K.M. Docherty, J.K. Dixon, C.F. Jr. Kulpa, Biodegradability of imidazolium and pyridinium ionic liquids by an activated sludge microbial community, Biodegradation 18 (2007) 481–493.
[16] F. Yebra, K. Zemánková, J. Troncoso, Speed of sound in ionic liquids with a common ion as a function of pressure and temperature, J. Chem. Thermodyn. 116 (2018) 235–240.
[17] J. Safarov, R. Hamidova, S. Zepik, H. Schmidt, I. Kul, A. Shahverdiyev, E. Hassel, Thermophysical properties of 1—hexyl—3—methylimidazolium bis (trifluoromethyl-sulfonyl)imide at high. Temperatures and pressures, J. Mol. Liq. 187 (2013) 137–156.
[18] J. Safarov, M. Geppert-Rybczyńska, I. Kul, E. Hassel, Thermophysical properties of 1—butyl—3—methylimidazolium acetate over a wide range of temperatures and pressures, Fluid Phase Equilib. 383 (2014) 144–155.
[19] A. Maghari, F. ZiaMajidi, Prediction of thermodynamic properties of pure ionic liquids through extended SAFT—BACK equation of state, Fluid Phase Equilib. 356 (2013) 109–116.
[20] A. Maghari, F. ZiaMajidi, E. Pashaei, Thermophysical properties of alkyl —imidazolium based ionic liquids through the heterosegmented SAFT—BACK equation of state, J. Mol. Liq. 191 (2014) 59–67.
[21] R. Hamidova, I. Kul, J. Safarov, A. Shahverdiyev, E. Hassel, Thermophysical properties of 1—butyl—3—methylimidazolium bis(trifluoromethylsulfonyl) imide at high temperatures and pressures, Braz. J. Chem. Eng. 32 (2015) 303–316.
[22] J.T. Safarov, A.T. Namazova, A. Shahverdyiev, E. Hassel, (p, ρ, T) properties of 1-octyl-3-methylimidazolium tetrafluoroborate, J. Serb. Chem. Soc. 83 (2018) 61–73.
[23] E. Zorębski, M. Zorębski, Comment on "Influence of temperature and pressure on the density and speed of sound of 2-hydroxyethylammonium propionate ionic liquid as well as N-ethyl-2-hydroxyethylammonium propionate ionic liquid", J. Chem. Thermodyn. 136 (2019) 149–151.
[24] S. Jężak, M. Dzida, M. Zorębski, High pressure physicochemical properties of 2-methylfuran and 2.5-dimethylfuran – second generation biofuels, Fuel 184 (2016) 334–343.
[25] M. Żarska, K. Bartoszek, M. Dzida, High pressure physicochemical properties of biodiesel components derived from coconut oil or babassu oil, Fuel 125 (2014) 144–151.
[26] M. Dzida, S. Jężak, J. Sumara, M. Żarska, P. Góralski, High pressure physicochemical properties of biodiesel components used for spray characteristics in diesel injection systems, Fuel 111 (2013) 165–171.
[27] M. Dzida, Speeds of sound, densities, isobaric thermal expansion, compressibilities, and internal pressures of heptan-1-ol, octan-1-ol, nonan-1-ol, and decan-1-ol at temperatures from (293 to 318) K and pressures up to 100 MPa, J. Chem. Eng. Data 52 (2007) 521–531.
[28] E. Zorębski, M. Dzida, The effect of temperature and pressure on acoustic and thermodynamic properties of 1,4-butanediol. The comparison with 1,2-, and 1,3-butanediols, J. Chem. Thermodyn. 54 (2012) 100–107.
[29] Q.-S. Liu, M. Yang, P.-F. Yan, X.-M. Liu, Z.-C. Tan, U. Welz-Biermann, Density and surface tension of ionic liquids $[C_npy][NTf_2]$ ($n = 2, 4, 5$), J. Chem. Eng. Data 55 (2010) 4928–4930.
[30] S. Zhang, X. Lu, Q. Zhou, X. Li, X. Zhang, S. Li, Ionic Liquids. Physicochemical Properties, Elsevier, Amsterdam, 2009.
[31] Q.S. Liu, M. Yang, P.P. Li, S.S. Sun, U. Welz-Biermann, Z.C. Tan, Q.G. Zhang, Physicochemical properties of ionic liquids $[C_3py][NTf_2]$ and $[C_6py][NTf_2]$, J. Chem. Eng. Data 56 (2011) 4094–4101.
[32] E.J. González, B. Gonzalez, E.A. Macedo, Effect of the relative humidity and isomeric structure on the physical properties of pyridinium based–ionic liquids, J. Chem. Thermodyn. 86 (2015) 96–105.
[33] J. Benito, M. Garcia–Mardones, V. Perez–Gregorio, I. Gascon, C. Lafuente, Physicochemical study of *n*–ethylpyridinium bis(trifluoromethylsulfonyl)imide ionic liquid, J. Solut. Chem. 43 (2014) 696–710.
[34] E. Zorębski, M. Zorębski, M. Dzida, Acoustic nonlinearity parameter B/A, internal pressure, and acoustic impedance determined at pressures up to 100 MPa for 1-ethyl-3-methylimidazolium bis(trifluoromethylsulfonyl)imide, Arch. Acoust. 41 (2016) 59–66.
[35] E. Zorębski, M. Musiał, M. Dzida, Relation between temperature-pressure dependence of internal pressure and intermolecular interactions in ionic liquids – comparison with molecular liquids, J. Chem. Thermodyn. 131 (2019) 347–359.
[36] E. Zorębski, Internal pressure as a function of pressure for alkanols, Mol. Quant. Acoust. 28 (2007) 319–326.
[37] M. Zorębski, E. Zorębski, M. Dzida, J. Skowronek, S. Jężak, P. Goodrich, J. Jacquemin, Ultrasonic relaxation study of 1-alkyl-3-methylimidazolium-based room-temperature ionic liquids: probing the role of alkyl chain length in the cation, J. Phys. Chem. B 120 (2016) 3569–3581.